The Astrophysical Journal, 956:22 (13pp), 2023 October 10 https://doi.org/10.3847/1538-4357/acf311

A High-level Ab Initio Study of the Destruction of Methanimine under UV Radiation

A. Bouallagui[1,2], A. Zanchet[2], M. Mogren Al Mogren[3], L. Bañares[4,5], and A. García-Vela[2]
[1] Laboratoire de Spectroscopie Atomique, Moléculaire et Applications (LSAMA) LR01ES09, Faculté des Sciences de Tunis, Université de Tunis El Manar, 2092, Tunis, Tunisia
[2] Instituto de Física Fundamental, CSIC, Serrano 123, E-28006 Madrid, Spain; garciavela@iff.csic.es
[3] Department of Chemistry, Faculty of Science, King Saud University, P.O. Box 2455, Riyadh 11451, Saudi Arabia
[4] Departamento de Química Física, Facultad de Ciencias Químicas, Universidad Complutense de Madrid (Unidad Asociada I+D+i CSIC), E-28040 Madrid, Spain
[5] Instituto Madrileño de Estudios Avanzados en Nanociencia (IMDEA-Nanoscience), Cantoblanco, E-28049 Madrid, Spain
Received 2023 April 20; revised 2023 August 21; accepted 2023 August 21; published 2023 October 4

Abstract

The photodecomposition of methanimine (CH_2NH) in the interstellar medium through several possible pathways is investigated by means of high-level multireference configuration interaction ab initio calculations. Among these pathways are photodissociation pathways involving hydrogen-atom elimination from both the CH_2 and NH groups, and fragmentation into CH_2 and NH. Potential-energy curves for the ground and several excited electronic states, as well as nonadiabatic couplings between them, are calculated. Possible dissociation mechanisms are discussed for the different pathways. It is found that the minimum excitation energy required for methanimine dissociation is above 7 eV. By using a two-dimensional representation of methanimine, $CH_2NH \rightarrow CHNH_2$ isomerization is explored as an additional methanimine decomposition pathway. Hydrogen-atom elimination from the CH_2 group is also investigated along the isomerization pathway. The results show that the isomerization proceeds by overcoming a transition state that in the first two excited states would require excitation energies similar to or somewhat lower than the typical minimum energies needed for breaking the molecule through the fragmentation pathways. Therefore, $CH_2NH \rightarrow CHNH_2$ isomerization can effectively contribute to methanimine decomposition, competing efficiently with the photodissociation pathways. The radiation content present in the interstellar medium makes possible the occurrence of all the pathways studied.

Unified Astronomy Thesaurus concepts: Complex organic molecules (2256); Photodissociation reactions (2266)

1. Introduction

Methanimine ($H_2C{=}NH$) is the simplest of the imines, which are molecules containing a carbon–nitrogen double bond. Formation of methanimine has been observed in the pyrolysis of methylamine (Peel & Willet 1975; Pearson & Lovas 1977) and of methyl azide (Bock & Dammel 1987, 1988). Methanimine has attracted remarkable astrophysical interest because it has been observed in dust clouds in the interstellar medium (ISM). It was first identified in gas phase in the molecular cloud Sagittarius (Sgr) B2 in the Galactic center (Godfrey et al. 1973). It has also been detected in the molecular cloud L183 (Turner et al. 1999), in Orion-KL (Dickens et al. 1997; White et al. 2003), at the edge of the Orion Bar photodissociation region (PDR; Cuadrado et al. 2017), in G19.61-0.23 (Qin et al. 2010), and in IRC+10216 (Tenenbaum et al. 2010). In addition, the Cassini T5 flyby has revealed an abundance of CH_2NH in Saturn's moon Titan (Vuitton et al. 2007). More recently, methanimine megamasers have also been detected in six galaxies hosting compact obscured nuclei (Zw 049.057, IRAS 17208-0014, IRAS 17578-0400, NGC 4418, IC 860, and Arp 220; Gorski et al. 2021).

Among the main aspects of the interest in the role of methanimine in the interstellar chemistry is the possibility that CH_2NH is a precursor in the formation of glycine, the simplest amino acid, in the ISM (Dickens et al. 1997; Danger et al. 2011; Chandra et al. 2016). Methanimine is also known to be a precursor of HCN and HNC products (Roithova et al. 2005; Larson et al. 2006). These species are ubiquitous molecules in the ISM, and they have been detected in diffuse clouds (Liszt & Lucas 2001), translucent molecular clouds (Turner et al. 1997), dark clouds (Hirota et al. 1998), star-forming regions (Loughnane et al. 2012), and circumstellar gas (Dutrey et al. 1997; Kastner et al. 1997). Thus, the presence and abundance of methanimine in the ISM, as well as its possible ways of decomposition (or disappearance), are of relevant interest to astrophysics. Photodissociation is one such way of decomposition for methanimine, and investigating its different mechanisms is the main goal of this work.

Most of the experimental studies on methanimine have been spectroscopic ones. The infrared spectrum of methanimine has been observed in argon matrix isolation (Milligan 1961; Jacox & Milligan 1975), and in the gas phase (Duxbury & Kato 1981; Hamada et al. 1984; Halonen & Duxbury 1985a, 1985b). The gas-phase structure has been determined by microwave spectroscopy (Pearson & Lovas 1977). The photoelectron spectra of CH_2NH have also been obtained (Bock & Dammel 1987, 1988). More recently, the electronic spectrum associated with the transition $\tilde{A}\ ^1A'' \leftarrow \tilde{X}\ ^1A'$ has also been measured (Teslja et al. 2004). Also recently, the formation of methanimine in the ISM has been explored in the laboratory, demonstrating that it can be synthesized by exposing low-temperature (5 K) interstellar model ices of CH_3NH_2 to ionizing radiation like energetic electrons (Zhou et al. 2019).

Experimental works on the fragmentation of methanimine are rather scarce, and typically restricted to sequential unimolecular fragmentation of the N–H bond and one C–H bond to form HCN + 2H products, and to unimolecular decomposition to produce HNC + H_2 fragments. In these cases

methanimine is an intermediate molecule produced by photolysis of other precursors like methylamine (CH_3NH_2; Roithova et al. 2005), or methyl azide (CH_3N_3; Larson et al. 2006). In the above cases, however, fragmentation of methanimine is not produced by photoexcitation. Actually, to the best of our knowledge no experimental works on photodissociation of methanimine have been reported.

Theoretical studies of methanimine are more abundant in the literature than experimental ones. Several ab initio (Ditchfield et al. 1972; MaCaulay et al. 1973; Cimiraglia & Tomasi 1977; Kitaura et al. 1978; Osamura et al. 1979; Demuynck et al. 1980; McPherson et al. 1983; Pople et al. 1983; Bonacic-Koutecky & Michl 1985; Bruna et al. 1985; Nguyen 1985; Richards et al. 1994; Nguyen et al. 1996; Sumathi 1996; Arenas et al. 1999; Zhou & Schlegel 2009) and density functional theory (Chestnut 2001) calculations on methanimine have been reported in the last several decades. In most cases those works calculated stationary points, e.g., the minima of the ground and low-lying excited states of methanimine and its fragmentation products, and the transition states connecting them, in order to investigate the vertical electronic spectrum of methanimine (MaCaulay et al. 1973; Bruna et al. 1985), the isomerization process $CH_3N \rightarrow CH_2NH$ (Demuynck et al. 1980; McPherson et al. 1983; Pople et al. 1983; Nguyen 1985; Richards et al. 1994; Sumathi 1996; Arenas et al. 1999; Zhou & Schlegel 2009), and methanimine dissociation to form HCN and HNC (Nguyen et al. 1996; Arenas et al. 1999; Zhou & Schlegel 2009). The dissociation dynamics of neutral methanimine as well as of the monocation and of the dication were investigated in the ground electronic state by means of ab initio direct classical trajectory calculations (Zhou & Schlegel 2009). In general, no potential-energy curves (PECs) or potential-energy surfaces of electronic states of methanimine have been reported. One exception would be Bruna et al. (1985), where PECs for the ground and first excited electronic states were calculated for the dissociation pathway producing CH_2 and NH fragments.

The absence of PECs or potential-energy surfaces for the different (ground and excited) electronic states of methanimine makes it very difficult to investigate the photofragmentation dynamics of this molecule by methods different from those based on ab initio direct dynamics (as in Zhou & Schlegel 2009). For this purpose, information is required on the structure and dependence of the electronic states of methanimine along the dissociation coordinates associated with the different fragmentation pathways, as well as on the couplings between such states. Obtaining the above information in order to understand the photodissociation dynamics of methanimine is the main goal of the current work.

The possible fragmentation pathways of methanimine are

$$CH_2NH \rightarrow CH_2N + H, \quad (1)$$

$$CH_2NH \rightarrow trans{-}HCNH + H, \quad (2)$$

$$CH_2NH \rightarrow cis{-}HCNH + H, \quad (3)$$

$$CH_2NH \rightarrow CH_2 + NH, \quad (4)$$

$$CH_2NH \rightarrow HCN + 2H, \quad (5)$$

$$CH_2NH \rightarrow HNC + H_2. \quad (6)$$

In the present work fragmentation pathways (1)–(4) are investigated by means of multireference configuration interaction (MRCI) ab initio calculations. The PECs of the ground and several excited electronic states along the corresponding dissociation coordinates of the four pathways are calculated. Conical intersections (CIs) between different electronic states are identified, and in some cases the couplings associated with these CIs are computed. Likewise, nonadiabatic couplings between states leading to electronic predissociation are obtained. Investigation of pathways (5) and (6) requires us to consider several coordinates in the MRCI calculations, which is beyond the scope of the current work.

In addition to the PECs obtained for dissociation pathways (1)–(4), we use a two-dimensional representation consisting of the C–H dissociation coordinate and the angle between the vector associated with this coordinate and the C–N axis. Such representation allows us to investigate the H-atom elimination along the pathway of in-plane hydrogen migration from the C center to the N center of the molecule, associated with methanimine isomerization to aminocarbene ($CHNH_2$).

2. Methodology

The different fragmentation pathways of CH_2NH leading to $CH_2N + H$, HCNH (*cis* and *trans*) + H, and CH_2 + NH, as well as the isomerization process $CH_2NH \rightarrow CHNH_2$ in combination with H-atom elimination from the CH_2 group, were explored using high-level ab initio methods. Each pathway was studied individually, first on the ground state, where relaxed scans were performed at the CASPT2 level (Werner et al. 1996). The relaxed scans were performed by fixing the distance of each bond CH, NH, and CN between 0.5 and 5 Å, and for each distance, the remaining coordinates were optimized.

The exploration of isomerization combined with hydrogen-atom elimination was performed in a similar way, but in addition to the C–H distance, the NCH angle was also frozen, leading to a relaxed two-dimensional grid. To make the calculations more tractable, the system was always maintained in the same plane so that all calculations could be performed using the C_s symmetry. For each of the optimized geometries, the first nine electronic singlet states lying below the ionization threshold at the equilibrium geometry were computed at the MRCI level (Knowles & Werner 1992), four of them being of A' symmetry and five of A'' symmetry. In addition, four triplet electronic states (two A' and two A'') were also computed at the MRCI level for three of the dissociation channels using the same orbitals. The orbitals (see the Appendix) were obtained prior to the MRCI calculation using the state-average CASSCF method (Werner & Knowles 1985). To achieve the required stability of the orbitals in the active space along the different reaction pathways, only the nine singlet states were considered in the CASSCF treatment with an active space consisting of 12 electrons in 10 orbitals (seven a' and three a''), while the two first orbitals associated with the 1*s* orbital of nitrogen and carbon were always kept doubly occupied. We should remark that these two orbitals were kept frozen in the MRCI treatment. All calculations were performed using the aug-cc-pVTZ basis set of Dunning (1989) using the MOLPRO package.[1]

The transition dipole moment components (TDMs) were computed at the CASSCF level at the equilibrium geometry. From the TDMs, the corresponding oscillator strengths were

[1] Available online at "A package of ab initio Programs", http://www.molpro.net.

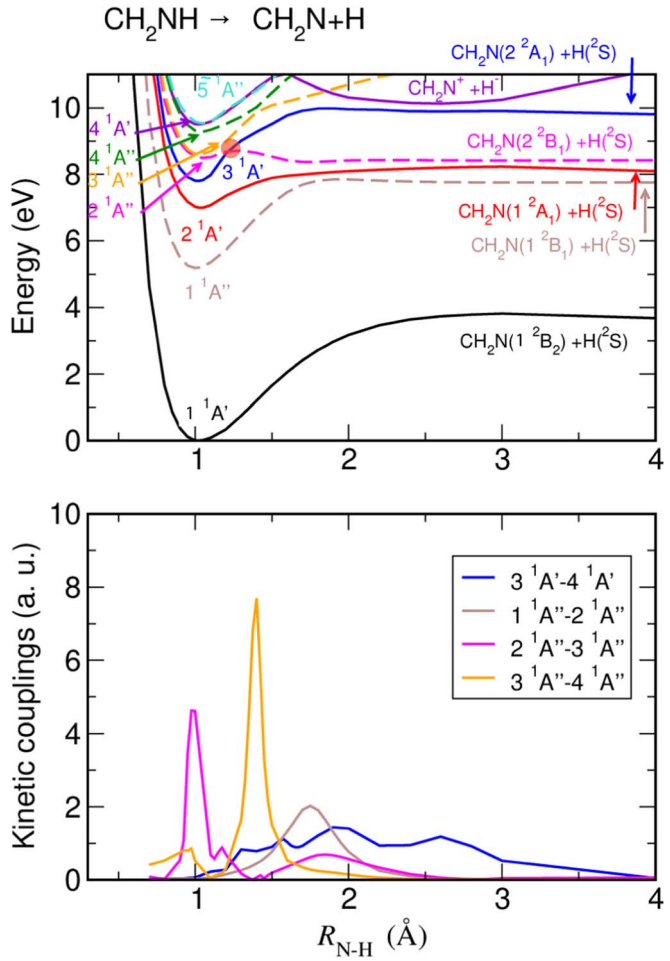

Figure 1. Upper panel: adiabatic PECs of the different electronic states along the N–H bond distance for the $CH_2NH \rightarrow CH_2N + H$ fragmentation pathway. The orange circle denotes a CI between the 3 $^1A'$ and 2 $^1A''$ states that is expected to occur upon leaving the plane of the C_s symmetry. Lower panel: calculated nonadiabatic couplings between some of the different electronic states.

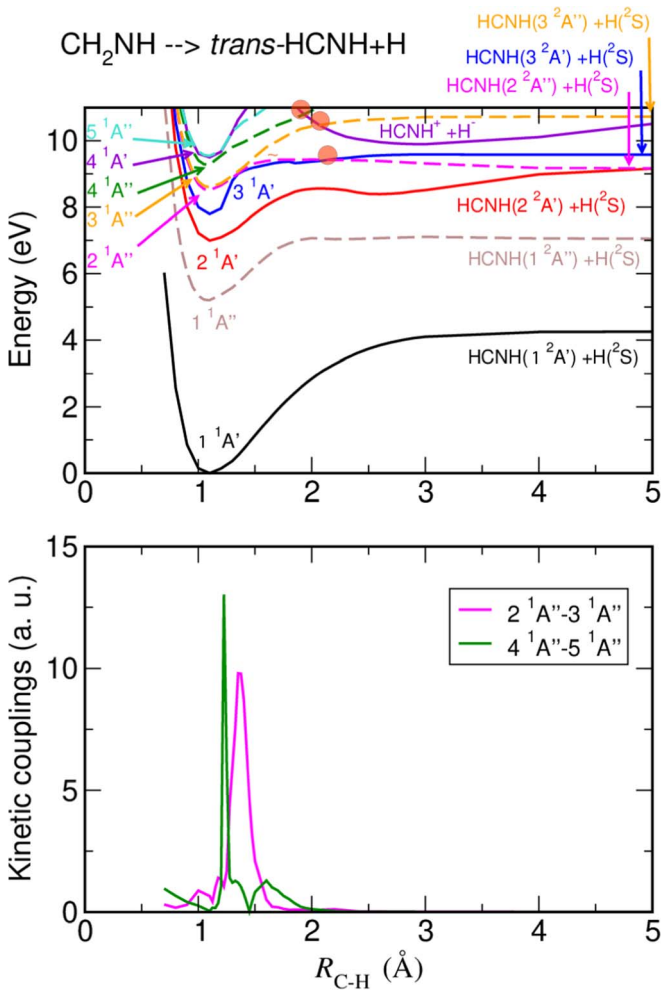

Figure 2. Upper panel: adiabatic PECs of the different electronic states along the C–H bond distance for the $CH_2NH \rightarrow$ *trans*-CHNH + H fragmentation pathway producing the CHNH fragment in the *trans* configuration. The orange circles denote CIs between the 3 $^1A'$ and 2 $^1A''$ states, 3 $^1A''$ and 4 $^1A'$ states, and 4 $^1A''$ and 4 $^1A'$ states that are expected to occur upon leaving the plane of C_s symmetry. Lower panel: calculated nonadiabatic couplings between some of the different electronic states.

calculated as (using atomic units)

$$f_{ij} = \frac{2}{3}(E_j - E_i)| < \Psi_i|\mathrm{TDM}|\Psi_j > |^2, \quad (7)$$

with i being the ground electronic state and j the corresponding excited state.

3. Results and Discussion

3.1. Fragmentation Pathways of Methanimine

Molecules like methanimine present different fragmentation pathways upon photoexcitation, depending on the specific bond of the molecule that is broken. A variety of dissociation mechanisms were found when different fragmentation pathways were recently investigated in alkyl radicals like ethyl, CH_3CH_2 (Chicharro et al. 2019, 2021; Marggi Poullain et al. 2019, 2022), and vinyl, CH_2CH (Bouallagui et al. 2022). Actually, due to the similarity between methanimine and vinyl (they only differ by the N and C atoms of the NH and CH groups, respectively), they present similar fragmentation pathways. The PECs of the different electronic states reported here for pathways (1)–(4) are intended to provide a guide for interpreting future excited-state dissociation experiments.

Figures 1–4 display the calculated ab initio PECs corresponding to the ground and first excited electronic states, along with the associated nonadiabatic couplings between them for dissociation pathways (1)–(4), respectively. Before discussing the different dissociation pathways, we find it will be interesting to determine which excited states can be accessed from the ground state. For this purpose, the dipole moments and oscillator strengths associated with the transitions from the ground state to the first seven excited states were computed, and they are collected in Table 1. The table shows that actually all these states have nonzero oscillator strengths, and thus all of them can be populated. More specifically, the 2 $^1A''$ and 4 $^1A''$ states present the highest oscillator strengths, and the second (2 $^1A'$) and third (3 $^1A'$) excited states also have appreciable values.

Now we shall begin by discussing H-atom elimination pathways (1)–(3). The upper panel of Figure 1 displays the PECs corresponding to pathway (1), associated with H-fragment elimination from the NH group producing $CH_2N + H$ fragments. The nonadiabatic couplings shown in the lower panel of Figure 1 create exit barriers to dissociation in

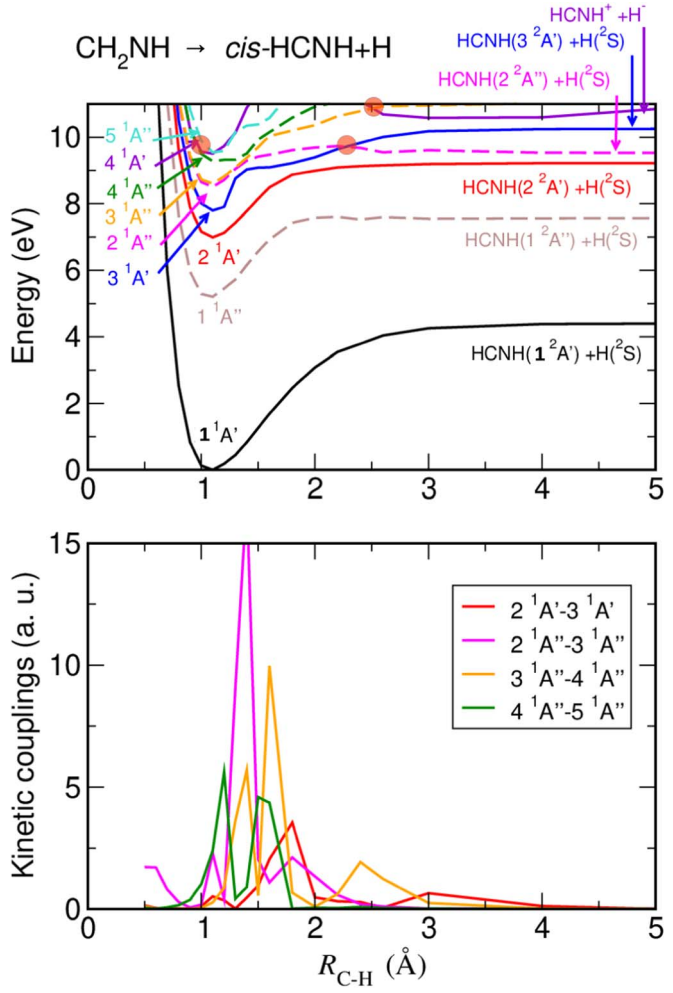

Figure 3. Upper panel: adiabatic PECs of the different electronic states along the C–H bond distance for the $CH_2NH \rightarrow$ *cis*-CHNH + H fragmentation pathway producing the CHNH fragment in the *cis* configuration. The orange circles denote CIs between the 3 $^1A'$ and 2 $^1A''$ states, 4 $^1A'$ and 5 $^1A''$ states, and 3 $^1A''$ and 4 $^1A'$ states that are expected to occur upon leaving the plane of C_s symmetry. Lower panel: calculated nonadiabatic couplings between some of the different electronic states.

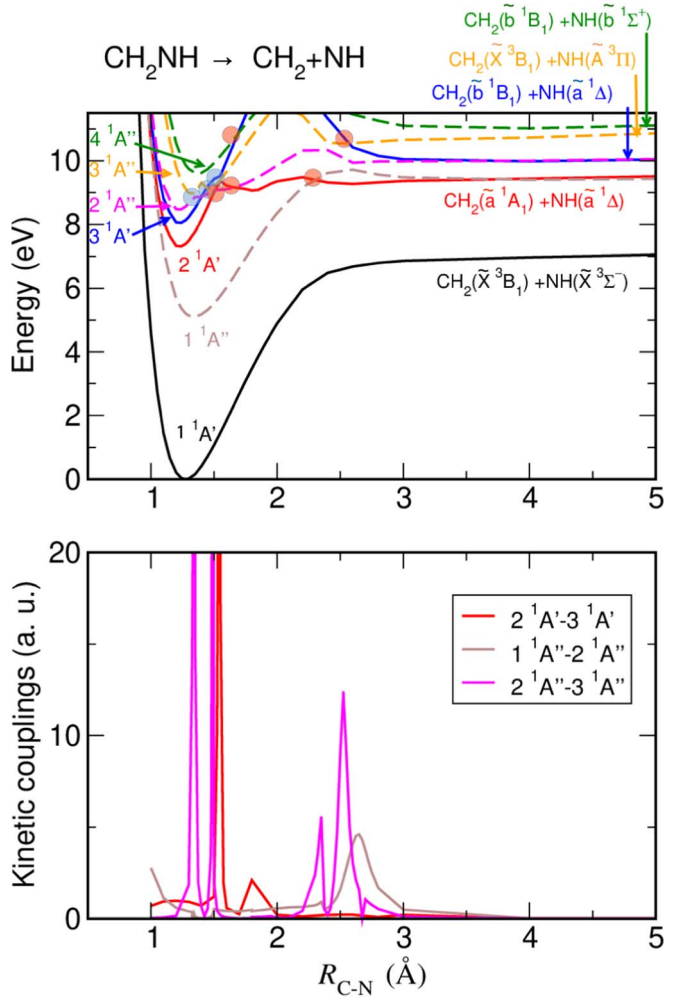

Figure 4. Upper panel: adiabatic PECs of the different electronic states along the C=N bond distance for the $CH_2NH \rightarrow CH_2 + NH$ fragmentation pathway. The blue circles denote the CIs identified within the planar C_s symmetry, one between the 2 $^1A'$ and 3 $^1A'$ states, and two between the 2 $^1A''$ and 3 $^1A''$ states. The orange circles denote CIs between states of different symmetries—namely two between the 2 $^1A'$ and 2 $^1A''$ states, and one between the 1 $^1A''$ and 2 $^1A'$ states, the 3 $^1A'$ and 3 $^1A''$ states, and the 3 $^1A'$ and 4 $^1A''$ states—that are expected to occur upon leaving the plane of C_s symmetry. Lower panel: calculated nonadiabatic couplings between some of the different electronic states, which include the couplings associated with the three CIs marked by the blue circles, and the couplings leading to electronic predissociation. The intensity of the three CI couplings has been cut in order to facilitate visualization of the remaining couplings.

some of the excited states, due to avoided crossings with other electronic states. It is noted, however, that such barriers are rather low in general. No CIs between electronic states are found within the planar C_s symmetry assumed in the present calculations. One CI (indicated by the orange circle) is identified between the states 3 $^1A'$ and 2 $^1A''$ of different symmetries within the C_s symmetry. This CI between different symmetry states is expected to occur upon leaving the plane of C_s symmetry.

The PECs of Figure 1 display a large energy separation between the ground and excited electronic states. The minimum of the first excited state 1 $^1A''$ is at around 5.2 eV. The spectrum measured for the 1 $^1A'' \leftarrow$ 1 $^1A'$ electronic transition (the *A* band; Teslja et al. 2004) between 234 and 260 nm (i.e., between 4.77 and 5.3 eV) exhibits a maximum at 249 nm or 4.98 eV. Thus, the agreement of the vertical excitation energy of ~5.2 eV between our calculated PECs of the 1 $^1A'$ and 1 $^1A''$ states with the experimental spectrum is very good. Since the 1 $^1A'$ and 1 $^1A''$ states are far away in energy from each other, only radiative coupling is expected between them, and then upon excitation to 1 $^1A''$ the only likely mechanism is relaxation to the ground state via fluorescence. Based on the PECs of Figure 1, internal conversion from 1 $^1A''$ to the ground state is not possible in the N–H stretching mode,

Table 1
TDMs and Oscillator Strengths (f) for Excitation from the Ground State to Several Excited Electronic States of CH_2NH

State	TDM_x (D)	TDM_y (D)	TDM_z (D)	f
1 $^1A''$	0	0.52	0	0.04
2 $^1A'$	0.30	0	0.85	0.14
3 $^1A'$	0.94	0	0.04	0.17
2 $^1A''$	0	1.54	0	0.50
3 $^1A''$	0	0.22	0	0.01
4 $^1A''$	0	0.23	0	0.39
4 $^1A'$	0.13	0	1.29	0.01

but it might be possible through couplings involving other modes. Figure 1 shows that the minimum of the second excited state 2 $^1A'$ is at 7 eV, while its asymptote is slightly above 8 eV, and the asymptote of the 1 $^1A''$ state is slightly below 8 eV. This implies that most of the potential well of 2 $^1A'$ (the region below the asymptote of 1 $^1A''$) is embedded in the well of 1 $^1A''$, and then most of the rovibrational states of 2 $^1A'$ are coupled to the highly excited ones of 1 $^1A''$. Thus, excitation of 2 $^1A'$ below 8 eV would cause relaxation by internal conversion to 1 $^1A''$, while dissociation in 2 $^1A'$ as well as in 1 $^1A''$ would require excitation above 8 eV (with wavelengths <155 nm). A nonadiabatic coupling between 1 $^1A''$ and 2 $^1A''$ (see lower panel of Figure 1) makes possible transitions between these two states (probably involving dissociation on the 2 $^1A''$ state), although it is likely that such coupling operates at excitation energies above 8 eV. Thus, high excitation energies around 8–9 eV (with 155–138 nm) would be required in order to produce excited $CH_2N(1\ ^2B_1)$, $CH_2N(1\ ^2A_1)$, and $CH_2N(2\ ^2B_1)$ fragments. Interestingly, at energies above 10 eV the $\tilde{G}$ $^1A'$ electronic state exhibits a shape characteristic of an ionic pair for distances $R_{N-H} < 1.5$ Å, likely due to charge transfer producing CH_2N^- and H^+ fragments.

In Figures 2 and 3 the PECs and some nonadiabatic couplings between them associated with pathways (2) and (3), respectively, are shown. Actually, the PECs corresponding to H-atom elimination producing *trans*- and *cis*-HCNH fragments display a rather similar shape. However, compared to that for pathway (1), the energy separation between the asymptotes of the ground and first excited states is remarkably smaller for pathway (2). The shape, depth, and dissociation limit of the 1 $^1A''$ state in pathway (3) are very similar to those of the corresponding state in pathway (1). The implication is that dissociation of methanimine through H-atom elimination in the first excited state is favored at lower excitation energies in pathway (2), compared to pathways (1) and (3). Another difference from pathway (1) is that the dissociation limit of the 2 $^1A'$ state is located about 1 eV higher for pathways (2) and (3). Thus, dissociation in the second excited state through pathways (2) and (3) would require correspondingly higher excitation energies.

Despite the above differences between the PECs of pathway (1) and those of pathways (2) and (3), there are some similarities between the three pathways leading to H-atom elimination. As in pathway (1), in pathways (2) and (3) the ground-state asymptote is located around 4 eV (4.2 eV for pathway (2) and 4.4 eV for pathway (3)). In the three cases, access to electronic states higher than the first excited one involves excitation energies above 7 eV, and the asymptote of the first excited state is also above 7 eV. This implies that for excitation below this energy, the expected mechanism for the three pathways would be radiative decay by fluorescence from 1 $^1A''$ to the ground state. The PECs of Figures 1–3 show in general excited states with rather shallow wells and low exit barriers, and no CIs are identified within the planar C_s symmetry. CIs are found only when the C_s symmetry is lifted by leaving the planar geometry, and these CIs lie at high energies, above 9 eV. Thus, high-energy excitation above 8–9 eV is expected to lead to rather fast dissociation favored by the low barriers, and also by transitions between excited states produced through the CIs when methanimine becomes nonplanar. Another common feature of pathways (1)–(3) is the ionic pair character apparently shown by the 4 $^1A'$ electronic state.

As mentioned above, the PECs associated with pathways (2) and (3) display a similar shape, in general. They also present two possible similar CIs outside the planar C_s symmetry (also at similar R_{C-H} distances): those between the 3 $^1A'$ and 2 $^1A''$ states and between the 3 $^1A''$ and 4 $^1A'$ states. There are, however, a few remarkable differences. One of them is that in Figure 2 a CI appears between the 4 $^1A''$ and 4 $^1A'$ states near $R_{C-H} = 2$ Å, while in Figure 3 a different CI occurs at shorter distances (around $R_{C-H} = 1$ Å) between the 4 $^1A'$ and 5 $^1A''$ states. Another difference is the larger (double) number of nonadiabatic couplings with appreciable intensity identified for the fragmentation pathway leading to the *cis*-HCNH product. The couplings between the 2 $^1A'$ and 3 $^1A'$ states and the 3 $^1A''$ and 4 $^1A''$ states reach a remarkably lower intensity in pathway (2). These additional intense couplings in pathway (3) cause avoided crossings between the corresponding PECs (clearly visible in Figure 3 in contrast to their absence in Figure 2), in the region around the maximum coupling intensity. They also contribute to the somewhat different shape of some of the excited PECs of the two pathways. A larger number of intense nonadiabatic couplings favor additional transitions between the different electronic states, leading to a larger variety of dissociation mechanisms in pathway (3) as compared to pathway (2). More specifically, the avoided crossings produced by the additional nonadiabatic couplings are likely to favor electronic predissociation mechanisms between the coupled states in pathway (3). As a result of these mechanisms, a larger production of *cis*-HCNH photofragments in the 2 $^1A'$ and 3 $^1A'$ states (HCNH(2 $^2A'$) and HCNH(3 $^2A'$), respectively) and in the 3 $^1A''$ and 4 $^1A''$ states (HCNH(3 $^2A''$) and HCNH(4 $^2A''$), respectively) is expected in pathway (3) with respect to pathway (2).

The PECs associated with pathway (4) are displayed in Figure 4 along with the nonadiabatic couplings found between different electronic states. The main difference from the PECs of pathways (1)–(3) is that the ground state 1 $^1A'$ of methanimine in Figure 4 is much deeper, and thus its asymptote is located at a remarkably higher energy (∼7 eV), closer to the asymptotes of the excited states. This situation is very similar to that found in the vinyl radical for the related dissociation pathway $CH_2CH \rightarrow CH_2 + CH$ (Bouallagui et al. 2022). This is not surprising, because in both vinyl and methanimine, the fragmentation of the C–C and C–N bonds, respectively, implies the breaking of a double bond.

The well of the first excited state of methanimine (1 $^1A''$) in Figure 4 is also deeper and the PEC displays a higher asymptote (located above 9 eV) than in pathways (1)–(3). The result that the asymptotes of the first and second excited states (1 $^1A''$ and 2 $^1A'$) are both located around 9.5 eV implies that below this energy (i.e., for excitation wavelengths >131 nm) only internal conversion from 2 $^1A'$ to 1 $^1A''$, and/or radiative decay from 2 $^1A'$ and 1 $^1A''$ to the ground state is possible. It is noted that due to the larger depth and higher asymptote of the ground state, in this pathway internal conversion from the 1 $^1A''$ state to highly excited rovibrational states of the ground state is also possible, in contrast to the case of the previous pathways. This internal conversion is expected to be a slow process due to unfavorable overlap between the low rovibrational states of 1 $^1A''$ and the highly excited ones of the ground state. After population of these excited rovibrational states at energies

above 5 eV, dissociation of CH_2NH in the ground electronic state is possible through pathways (1)–(3) (producing CH_2N, *trans*-HCNH, or *cis*-HCNH fragments), since for those pathways the ground-state asymptote is around 4 eV, below the energy of the rovibrational states excited (see Figures 1–3). Another difference from pathways (1)–(3) is that in the PECs of Figure 4 three CIs are identified within C_s symmetry (blue circles in the upper panel), one between the 2 $^1A'$ and 3 $^1A'$ states, and two between the 2 $^1A''$ and 3 $^1A''$ states. Up to five CIs between states of different symmetries (orange circles) are also identified. All these high-lying CIs are expected to favor fast transitions between excited states and dissociation of methanimine when the initial excitation occurs above 8–9 eV. Due to the high-lying dissociation limits of the ground and first excited states, the high excitation energies required make this pathway less favorable for photodissociation, and therefore for the disappearance of methanimine, than pathways (1)–(3).

It will be interesting to discuss now the six nonadiabatic couplings shown in Figures 1–4 for the different dissociation pathways, and the mechanisms in which they are involved. Some of the couplings appear in more than one pathway. The coupling between the 3 $^1A'$ and 4 $^1A'$ states in pathway (1) spreads over a large N–H distance range. Upon excitation to 4 $^1A'$, this coupling is likely to cause relaxation by internal conversion to highly excited vibrational states of 3 $^1A'$, and further dissociation in 3 $^1A'$. The coupling between the 2 $^1A''$ and 3 $^1A''$ states is interesting because it is present in the four pathways with different shapes. In pathways (1) and (2) the coupling presents two peaks, one around 1 Å and a broader one around 2 Å (although in pathway (2) this peak is very weak). In pathway (3) there is a third, smaller peak near 1 Å. In pathway (4) there are four peaks, two peaks very narrow and intense at distances <1.6 Å, associated with two CIs, and two smaller peaks around 2.5 Å. Leaving aside the two peaks associated with CIs, in the four pathways, the peaks at distances <1.6 Å are likely to produce transitions by internal conversion from 3 $^1A''$ to 2 $^1A''$, while the peaks at distances >1.6 Å produce avoided crossings that will lead to predissociation between the two states. Thus, upon excitation to these two states, and depending on the excitation energy, internal conversion from 3 $^1A''$ to 2 $^1A''$, followed by dissociation in 2 $^1A''$ in some cases, and/or predissociation from one state to the other, can occur.

The remaining four nonadiabatic couplings have in common that they appear only in two different pathways. The coupling between 1 $^1A''$ and 2 $^1A''$ appears in pathways (1) and (4) with a similar shape but at different bond distances (at ∼1.75 Å in pathway (1) and at ∼2.7 Å in pathway (4)). This coupling causes a relatively localized avoided crossing, which is expected to produce electronic transitions by electronic predissociation between the two states. The coupling connecting the 3 $^1A''$ and 4 $^1A''$ states is present in pathways (1) and (3). In pathway (1) this coupling displays two peaks, a small one around 1 Å and a larger one at ∼1.4 Å, while in pathway (3), in addition to these two peaks (appearing at somewhat larger bond distances) there is a third peak around 2.4 Å. The first peak at the shortest distance in the two pathways is likely to produce internal conversion from the upper state, while the peaks at larger distances in both pathways cause avoided crossings that will lead to predissociation between the states. The coupling between the 4 $^1A''$ and 5 $^1A''$ states occurs in pathways (2) and (3), and has a similar shape in both cases, namely two peaks near 1 and 1.5 Å. Only the relative intensity of the two peaks changes in the two pathways. As in several of the couplings previously discussed, the peaks at shorter bond distance will cause internal conversion from the upper state, while the second peak is associated with an avoided crossing producing predissociation between the electronic states. Finally, the coupling between the 2 $^1A'$ and 3 $^1A'$ states occurs in pathways (3) and (4). In pathway (3) there is a very small peak near 1 Å that appears to cause internal conversion from 3 $^1A'$. The narrow and very intense peak appearing around 1.5 Å is associated with a CI. A second, small peak near 2 Å appears for both pathways (3) and (4), which is associated with an avoided crossing and would cause predissociation between the states. Thus, upon excitation of electronic states above the second excited one, the combination of the above nonadiabatic couplings with the CIs leads to a rich and complex variety of dynamical mechanisms producing fragmentation and therefore decomposition of methanimine.

While this work focuses on the singlet excited electronic states of methanimine, because they are the ones that can be directly accessed radiatively from the ground state, we investigate the possible effect of including the first triplet excited states. For this purpose, we also calculate the first four excited triplet states for pathways (1), (2), and (4) (at the MRCI level), and they are shown along with all the calculated singlet states in Figure 5. As discussed above, the shapes of the PECs of the singlet states of pathways (2) and (3) are found to be very similar. We can thus expect a similar situation for the triplet states, and we calculate only the triplet PECs associated with pathway (2). Figure 5 shows that some of the singlet states cross with the triplet states for all the dissociation pathways. One interesting feature is an avoided crossing occurring at a short bond distance between the states 1 $^3A'$ and 2 $^3A'$ for pathways (1) and (2). In addition, the 1 $^3A'$ state correlates asymptotically with the same product fragments as the ground electronic state.

Since the triplet states cannot be accessed directly from the singlet ground state, the only way to populate them is by excitation of a singlet electronic state, followed by a mechanism of intersystem crossing (ISC) from that state to a triplet state coupled to it. Thus, the probability of such an ISC mechanism will depend on the intensity of the spin–orbit couplings between the singlet and triplet states. The couplings found between the first two n $^1A'$ (n = 2, 3) excited states with the first four triplet states are rather low (Orozco-Gonzalez et al. 2012). They are typically in the range 0–8.6 cm^{-1}, and only the coupling between 2 $^1A'$ and 1 $^3A''$ reaches 14.8 cm^{-1}, which is still weak. Regarding the couplings between the n $^1A''$ (n = 1–3) excited states and the triplet states, they are also low, typically ranging between 0 and 9.1 cm^{-1}. Only the couplings of 1 $^1A''$ and 2 $^1A''$ with 2 $^3A'$ are somewhat higher, being 23.6 and 25.2 cm^{-1}, respectively. Therefore, the spin–orbit couplings found between the singlet and first four triplet excited states are rather weak.

It will be interesting to discuss now whether including the first excited triplet states changes significantly the dynamical mechanisms discussed above when considering only the singlet states. The couplings between the excited singlet states and the two highest triplet states, 2 $^3A'$ and 2 $^3A''$, are typically weak, <8.6 cm^{-1}, except for the cases of 1 $^1A''$ and 2 $^1A''$, for which they are somewhat higher (23.6 and 25.2 cm^{-1}), as stated above. Thus, a very slow ISC process from the singlet states to

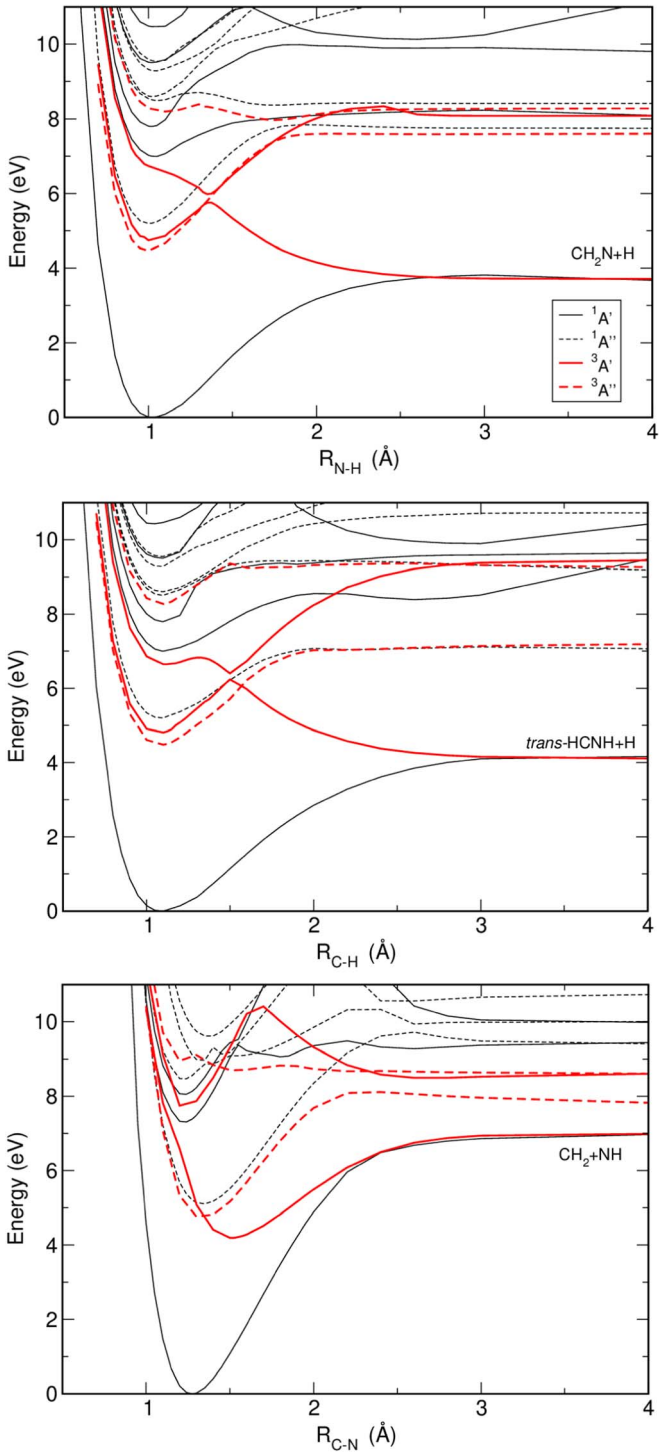

Figure 5. Adiabatic PECs along three fragmentation pathways for all the singlet electronic states shown in Figures 1, 2, and 4, and the first four triplet electronic states (1 $^3A''$, 1 $^3A'$, 2 $^3A'$, and 2 $^3A''$, following the order of energy). Upper panel: $CH_2NH \rightarrow CH_2N + H$ fragmentation pathway. Middle panel: $CH_2NH \rightarrow$ *trans*-HCNH + H fragmentation pathway. Lower panel: $CH_2NH \rightarrow CH_2 + NH$ fragmentation pathway.

these two triplet ones may occur. The PEC of 2 $^3A''$ presents a very shallow well (for pathways (1) and (2)) or is practically dissociative (for pathway (4)), so dissociation is expected in this state for excitation energies above its asymptote (>8–9 eV). The state 2 $^3A'$ is a bound one, so internal conversion to the lower 1 $^3A''$ state is likely for pathways (1) and (2), while dissociation by tunneling through the exit barrier can occur for pathway (4) for excitation energies >8.5 eV.

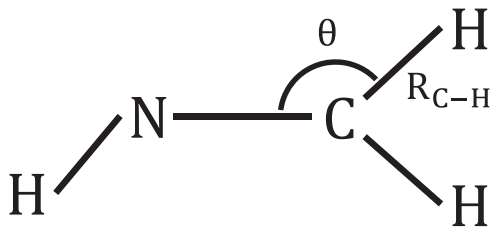

Figure 6. Scheme of the Jacobi coordinates R_{C-H} and θ used in the two-dimensional representation of methanimine, and associated with the H-atom migration leading to isomerization to aminocarbene, $CHNH_2$.

Weak couplings $\leqslant 14.8$ cm^{-1} are also found between the singlet states and the lowest triplet states 1 $^3A''$ and 1 $^3A'$, inducing a slow ISC process as well. After ISC, internal conversion between the two triplet states is likely to occur, combined with tunneling through the barrier of the 1 $^3A'$ state for pathways (1) and (2). For pathway (4), in addition to the internal conversion between both triplet states, a slow ISC (also mediated by weak couplings) to excited rovibrational states of the ground singlet state may occur. This latter ISC mechanism would be similar to the internal conversion expected for pathway (4) from 1 $^1A''$ to the ground state already mentioned. In summary, the inclusion of the first excited triplet states does not change significantly the dynamical mechanisms found previously considering only the singlet states. The mechanisms of ISC and dissociation by tunneling involving the triplet states appear to be slow enough due to the weak couplings with the singlets, that radiative relaxation by fluorescence from the excited singlet states to the ground state is probably faster.

3.2. Two-dimensional Representation of Methanimine Photoisomerization

In addition to hydrogen elimination from either the CH_2 or NH group, or the breaking of the C=N bond, photoisomerization would be a possibility for the disappearance of methanimine. The in-plane migration of a hydrogen atom from the CH_2 group to the NH group produces isomerization of methanimine to aminocarbene, $CHNH_2$. Such hydrogen in-plane migration can be described by using the two-dimensional representation shown in Figure 6. In principle, the description of the $CH_2NH \rightarrow CHNH_2$ isomerization process requires us to vary the angle θ in a broad range, and to sample the R_{C-H} bond distance only in a relatively short range within the interaction region of the potential-energy surface. However, we choose to sample the R_{C-H} coordinate in a broad region as in Figures 2 and 3, which includes both the interaction and asymptotic regions. In this way, in addition to the $CH_2NH \rightarrow CHNH_2$ isomerization, we can investigate the process of H-atom elimination from the CH_2 group along the isomerization pathway. This provides information on how this dissociation pathway changes along the isomerization process, and in particular allows us to compare how this H-atom elimination occurs both in methanimine and in aminocarbene.

Thus the PECs corresponding to the ground and excited electronic states are calculated along the R_{C-H} coordinate for several θ in the range [20°, 180°]. Specifically, the values of the angles for which calculations are carried out range from 20° to 180° in steps of 10°. In Figure 7 the calculated PECs along R_{C-H} are displayed for different values of θ. It is noted that

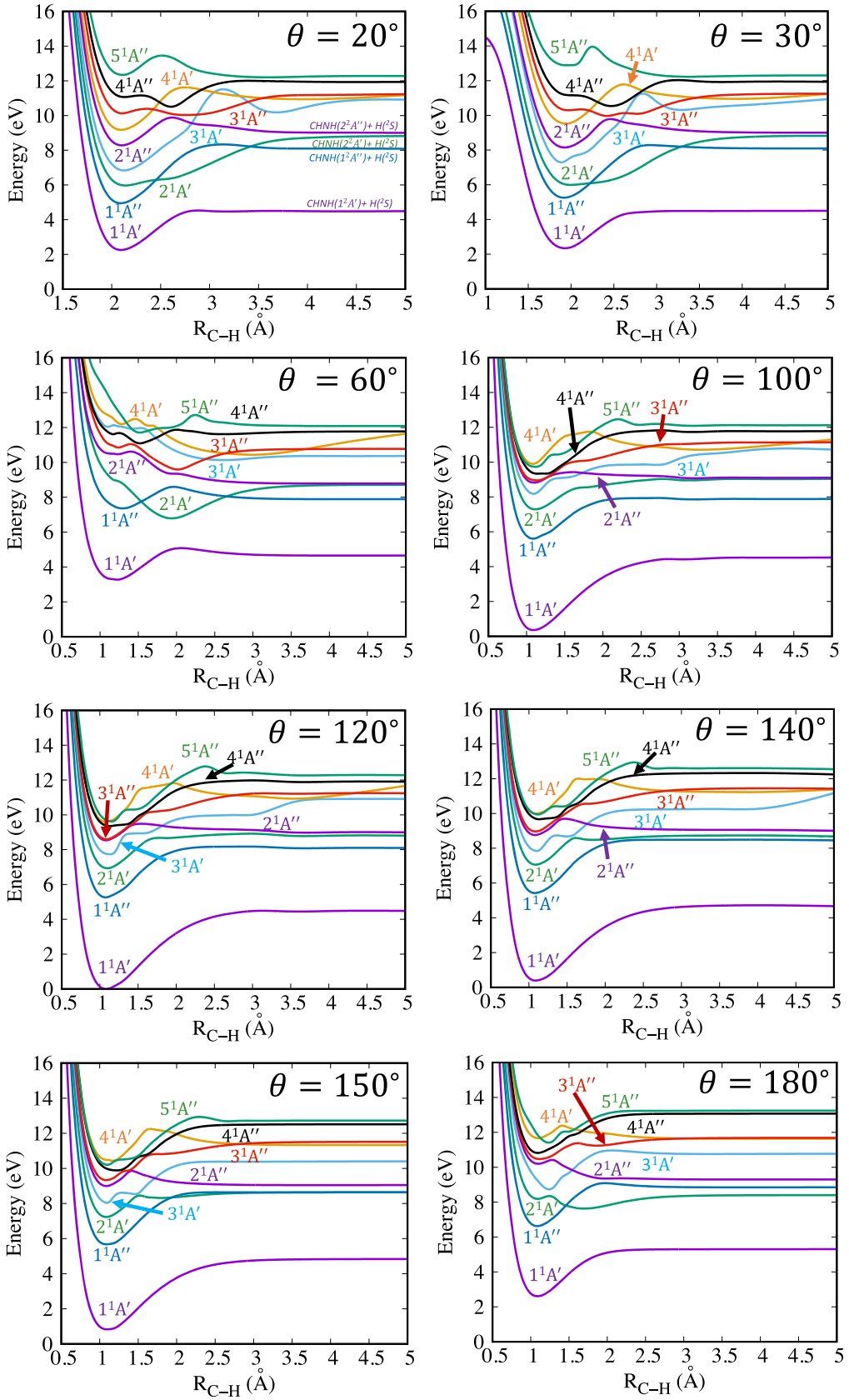

Figure 7. PECs calculated for the different electronic states along the R_{C-H} coordinate for several values of the angle θ (see Figure 6) in the range [0°, 180°].

since the H-atom migration leading to $CH_2NH \rightarrow CHNH_2$ isomerization proceeds in the molecular plane (see Figure 6), the C_s symmetry and the same active space used to calculate the PECs of Figures 1–4 can be conserved in the calculations of the PECs shown in Figure 7. Therefore, the PECs of Figure 7 are comparable to those of Figures 1–4.

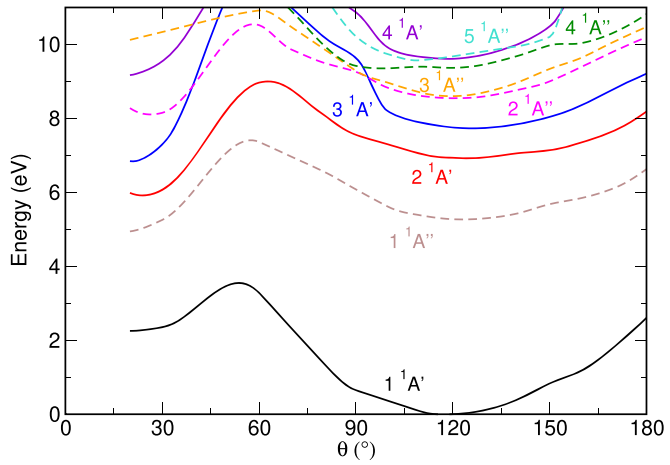

Figure 8. PECs of the different electronic states along the θ coordinate (see Figure 6). The curves are obtained by selecting the energy value of each state corresponding to the R_{C-H} distance for which the ground state $1\ ^1A'$ reaches the minimum energy at each angle θ.

The $CH_2NH \rightarrow CHNH_2$ isomerization process is clearly shown in Figure 7 by the evolution of the minima of the PECs (particularly that of the ground state) as the angle θ changes from $\theta = 180°$ to $\theta = 20°$. Indeed, as θ decreases from 180°, the global potential-energy minimum associated with methanimine occurs at $\theta = 120°$ and $R_{C-H} = 1.1$ Å. As θ decreases below 120°, the minimum of the different PECs becomes increasingly higher in energy, until reaching a transition state at around $\theta = 60°$. While the shape of the PECs changes gradually and not very much between $\theta = 180°$ and 100°, it is strongly affected at the transition state ($\theta = 60°$). In general the PECs display remarkably shallower wells, located at larger distances (as in the case of $2\ ^1A'$, $3\ ^1A'$, and $4\ ^1A''$). Even the minimum of the $2\ ^1A'$ well is lower in energy than that of the $1\ ^1A''$ state. By decreasing further the θ, the minima of the PECs gradually become lower in energy, in general, and the minimum energy associated with aminocarbene is reached around $\theta = 20°$, which completes the isomerization process. As expected, a distance $R_{C-H} = 2.1$ Å larger than that of the methanimine energy minimum is found for aminocarbene. The excited PECs of aminocarbene display high exit barriers to dissociation, in contrast to the situation of methanimine, where no barriers or rather low ones are found. Thus quite different photodissociation dynamics are expected in methanimine and aminocarbene.

The $CH_2NH \rightarrow CHNH_2$ isomerization is more clearly displayed by looking at the minimum energy pathway along θ, shown in Figure 8. As depicted in Figure 7, the curves of the different states display two minima around $\theta = 120°$ and $\theta = 20°$, and a transition state around $\theta = 60°$, reflecting the isomerization pathway. The ground electronic state of aminocarbene (see also the panel corresponding to $\theta = 20°$ in Figure 7) is remarkably less stable than that of methanimine. Indeed, while both ground states have a similar asymptote, slightly above 4 eV, the minimum energy of aminocarbene is about 2 eV higher, which results in a substantially smaller well depth, as shown in the ground-state curve of Figure 8. For this reason, the ground and excited states are closer in energy in aminocarbene, implying that excitation from the ground state to the different excited states requires much less energy than in methanimine. In contrast to the situation of the ground state, where the well associated with methanimine is the deepest one, the excited states in Figure 8 display shallower wells associated with methanimine than those corresponding to aminocarbene. The barriers associated with the transition states appear to be also substantially lower in energy, in general, than those in the ground state. Indeed, the height of the barriers found in Figure 8 is 3.54, 2.15, 2.10, 4.41, 2.03, and 2.37 eV for the ground, $1\ ^1A''$, $2\ ^1A'$, $3\ ^1A'$, $2\ ^1A''$, and $3\ ^1A''$ states, respectively (i.e., only the $3\ ^1A'$ excited state exhibits a higher barrier than the ground state). The interesting implication is that $CH_2NH \rightarrow CHNH_2$ isomerization would be in general easier in the excited states, although it would require the photon energy needed to reach such states.

As mentioned above, the height of the transition state to be surmounted in the ground-state potential curve to make possible $CH_2NH \rightarrow CHNH_2$ isomerization is 3.54 eV. It is nearly impossible to surmount this barrier by thermal activation in the cold ISM. Likewise, overcoming the barrier by means of vibrational excitation is unlikely due to the very low infrared oscillator strengths for transitions to high vibrational states. Thus, methanimine isomerization appears more probable upon a photoinduced transition to an excited state.

As already commented, the isomerization barriers of the excited states are in general lower than that of the ground state. This is the case of the first and second excited states. Thus, excitation to any of these states at energies above the corresponding barrier would cause isomerization of methanimine. Following Figure 8, the required energies would be above 7.5 eV (reached with excitation wavelengths <165 nm) for the $1\ ^1A''$ state, and above 9 eV (<138 nm) for the $2\ ^1A'$ excited state.

However, the barriers to be surmounted could be lower if we consider the two-dimensional representation of R_{C-H} and θ instead of the one-dimensional picture of Figure 8. The curves of Figure 8 are obtained for a fixed R_{C-H} distance for which the ground state $1\ ^1A'$ reaches the minimum energy at each angle θ. But when the two coordinates are considered, as in Figure 7, we see in this figure that at $\theta = 60°$, where the transition state occurs for the different electronic states, the $2\ ^1A'$ state displays a minimum below 7 eV for $R_{C-H} \sim 2.0$ Å. The implication is the following. At the equilibrium angle $\theta = 120°$ the $2\ ^1A'$ state is excited from the ground state at energies above the 7 eV of the well minimum in order to reach a given vibrational state. Now, by increasing the C–H bond distance from nearly 1 Å to nearly 2 Å, the molecule can surmount the barrier by decreasing the angle θ reaching energies below 8 eV (see the panels corresponding to $\theta = 100°$ and $\theta = 60°$ in Figure 7), up to finally arriving at the aminocarbene minimum at $\theta = 20°$. Thus there would be no need to excite the $2\ ^1A'$ state at energies above 9 eV.

The implication of the above discussion is that isomerization of methanimine to aminocarbene in the first and second excited states would require excitation energies above 7–7.5 eV, which are similar to or even lower than the typical minimum energies required for fragmentation of the molecule through pathways (1)–(4). Thus, the $CH_2NH \rightarrow CHNH_2$ isomerization mechanism appears to be an additional and efficient disappearance pathway of methanimine that is likely to effectively compete with pathways (1)–(4). Additionally, the result commented above that photodissociation of aminocarbene is favored by a lower excitation energy due to a less deep ground-state well would lead to a lower probability of recovering methanimine through inverse $CHNH_2 \rightarrow CH_2NH$ isomerization, making

methanimine decomposition as definitive as in the case of photodissociation pathways (1)–(4).

It is noted that in the ISM locations where methanimine has been observed, ultraviolet radiation is usually present with enough frequency to make possible the excitation of methanimine to the first and second excited states, inducing further photodissociation through pathways (1)–(4) or photoisomerization. In particular, the edge of the Orion Bar PDR is a position irradiated with a very intense far-UV radiation field, about 10^4 times the mean interstellar field (Marconi et al. 1998). The photoproducts generated by the photoinduced processes investigated here for methanimine (CH_2N, *trans*-HCNH, *cis*-HCNH, CH_2, NH, and aminocarbene, all of them in different electronic states) contribute to increase their budget in the ISM. These products can further act as precursors and/or intermediates in other reactions in the ISM.

3.3. Astrophysical Implications

Actually, very little is known about the mechanisms of formation and destruction of methanimine in the ISM, particularly about the role of the photochemistry of methanimine in those mechanisms. Lavvas et al. (2008) applied a model to predict the complex photochemistry in the atmosphere of Titan. The model predicted an amount of methanimine in Titan's atmosphere larger than that observed (Lavvas et al. 2008; Vuitton et al. 2014). This discrepancy between the amount of methanimine predicted and observed implies an underestimation of methanimine loss in the model. The model included the methanimine photodissociation reaction $CH_2NH + h\nu \rightarrow HCN + 2H$, using the associated rate constants calculated by Nguyen et al. (1996), and the absorption cross sections measured for the $1\ ^1A'' \leftarrow 1\ ^1A'$ transition (Teslja et al. 2004). Actually, the rate constants of Nguyen et al. (1996) correspond to several dissociation processes of methanimine by thermal decomposition in the ground electronic state, and not to the above methanimine photodissociation reaction considered in the model. This fact could contribute to the above discrepancy between the predicted and the observed amount of methanimine in Titan's atmosphere. The present work demonstrates that there are pathways of destruction of methanimine in addition to formation of HCN. It is noted that incident light with photon energy in the range 5–10 eV, required to photodissociate methanimine through those pathways, is available in different regions of Titan's atmosphere (Lavvas et al. 2009, 2011; Vuitton et al. 2014). Such additional pathways could contribute to lowering the budget of methanimine in the Titan atmosphere.

The fact that methanimine is observed in strongly irradiated regions may lead us to think that this molecule might be photoresistant to a large extent. After electronic excitation, methanimine may undergo fluorescence to the ground state, which would preserve the system against dissociation and destruction. This would have strong implications for the photochemistry network of the Titan atmosphere (Vuitton et al. 2014). Indeed, we can consider two possible scenarios. One of them is a high resistance to photodestruction, where UV photons cannot account for the loss of methanimine (except in cases of ionization, not studied here). The implication is that the only possible destruction pathways would be chemical reactions or collisions with electrons. However, methanimine is a stable closed-shell molecule, and it is not expected to react efficiently in its ground state. One possibility proposed by Vuitton et al. (2014) is reactive collisions with ionized molecules (cations), quite abundant in Titan's atmosphere. Another possibility would be chemical reactions involving electronically excited methanimine, since molecules in an electronic excited state are usually much more reactive. Due to the fact that the gas density in the Titan atmosphere is high, electronically excited methanimine may have enough time to collide with another molecule before relaxing to the ground state, N_2 and CH_4 being the most abundant colliding partners. Little is known, however, about this kind of reactions, and they are not included in the models (excepted for excited atoms such as $N(^2D)$). But $CH_2NH^* + CH_4$ collisions could possibly play a role in the Titan atmospheric chemistry. Also, isomerization cannot be fully excluded, as collision with N_2 could easily stabilize a rovibrationally excited isomer.

Now, let us consider a scenario where photodestruction of methanimine would still be efficient enough to be relevant. This would be the situation if internal conversion and/or ISC can compete against fluorescence. Our present results show that excitation to the first two singlet excited states $1\ ^1A''$ and $2\ ^1A'$ involves the lowest-energy photons (5–7 eV), and that internal conversion to the ground state may occur, as in pathway (4) (see Figure 4). ISC to a triplet state (only partially discussed in this work) may also end up in the ground state (see the lower panel of Figure 5), although this process should be very slow. As discussed above, after this internal conversion (or ISC) to the ground state, the stronger C–N bond would not break, but the weaker N–H and C–H bonds could easily break (the C–H bond with more statistical probability since there are two C–H bonds versus one N–H bond), causing photodestruction of methanimine. So the most likely photoproducts would be CH_2N, effectively detected in Titan, and HCNH in its *trans* or *cis* form. The fact that none of these two isomers have been detected may suggest that methanimine is indeed photoresistant, or it may also be due to the fact that the spectroscopy of the HCNH isomers is not well known, preventing their identification. In the case where HCNH would effectively be produced, this would have a potential implication on the HCN/HNC ratio. Indeed, we know that the electron capture of the HCNH cation leads to both HCN and HNC at a ratio of 50%. Thus, the photodestruction of HCNH may be one of the missing keys to understanding the cyano–isocyano ratios in Titan, as well as in PDRs. More studies are necessary to answer these questions, and the present work may serve to stimulate future experiments on the excited-state photochemistry of methanimine.

4. Conclusions

Possible pathways for photodecomposition and disappearance of methanimine (CH_2NH) in the ISM are investigated by means of high-level MRCI ab initio calculations. Among the pathways explored are photodissociation pathways involving hydrogen-atom elimination from both the NH group, producing $CH_2N + H$, and the CH_2 group, yielding *trans*-HCNH and *cis*-HCNH products, as well as those involving the breaking of the CN bond to produce $CH_2 + NH$ fragments. PECs for the ground and several excited electronic states are calculated along the dissociating bond distance, as well as nonadiabatic couplings between different states. CIs connecting some excited states are identified. Possible dynamical mechanisms are discussed in light of the calculated potential curves for all the photodissociation pathways. Photodissociation of

methanimine typically implies relatively high amounts of excitation energy. More specifically, dissociation in the first and second excited states would require a minimum excitation energy of about 7 or 8 eV (from 177 to 155 nm). In the ISM, where methanimine is abundant, radiation of those frequencies is present, and thus the four photodissociation pathways are possible candidates for methanimine decomposition.

In addition to the above photodissociation pathways, the $CH_2NH \rightarrow CHNH_2$ isomerization mechanism in combination with hydrogen-atom elimination from the CH_2 group is investigated as a possible methanimine decomposition pathway. This isomerization is produced by an in-plane hydrogen migration from the CH_2 group to the NH one. The isomerization proceeds through a transition state with an associated barrier. It is found that surmounting this barrier in the first two excited states requires excitation energies similar to or even lower than the minimum ones needed to fragment the molecule through the dissociation pathways. The implication is that $CH_2NH \rightarrow CHNH_2$ isomerization is an additional pathway for methanimine decomposition that can effectively compete with the photodissociation pathways.

All the above photodestruction mechanisms are of course in competition against fluorescence, which preserves the system. Since high-energy photons (>7–8 eV) are necessary to access the photofragmentation pathways, the fact that methanimine may undergo fluorescence suggests that this molecule could exhibit photoresistance to a certain degree, explaining why it can be detected in strongly irradiated regions of the ISM. Even if methanimine is photoresistant to some extent, since all the photodestruction pathways investigated here are accessible with the UV frequencies present in irradiated ISM regions, where methanimine has been observed, they are expected to contribute to the modulation of the abundance of this molecule in such regions. In order to quantify the relative efficiency of the possible mechanisms, experimental studies on the photodissociation and fluorescence of this system would be required.

Acknowledgments

This research has been carried out within the Unidad Asociada Química Física Molecular between the Departamento de Química Física of Universidad Complutense de Madrid and CSIC. This work was funded by the Ministerio de Ciencia e Innovación (MICINN, Spain), grant Nos. PGC2018-096444-B-I00, PID2019-107115GB-C21, PID2021-122549NB-C21, PID2021-122796NB-I00, and PID2021-122839NB-I00. A.B. acknowledges funding from the I-COOP program from CSIC, grant No. COOPB20364, which made possible a research stay at Instituto de Física Fundamental, CSIC. This project has received funding from the European Union's Horizon 2020 research and innovation program under Marie Skłodowska-Curie Grant Agreement No. 872081. The authors acknowledge the National Plan for Science, Technology and Innovation (MAARIFAH), King Abdulaziz City for Science and Technology, Kingdom of Saudi Arabia, grant No. 2-17-01-001-0061. The Centro de Supercomputación de Galicia (CESGA, Spain) is acknowledged for allowing the use of its resources. We acknowledge fruitful discussions with N. Balucani, J. R. Goicoechea, and M. Agúndez.

Appendix

In Figure 9 the CASSCF state-average orbitals included in the active space used are displayed.

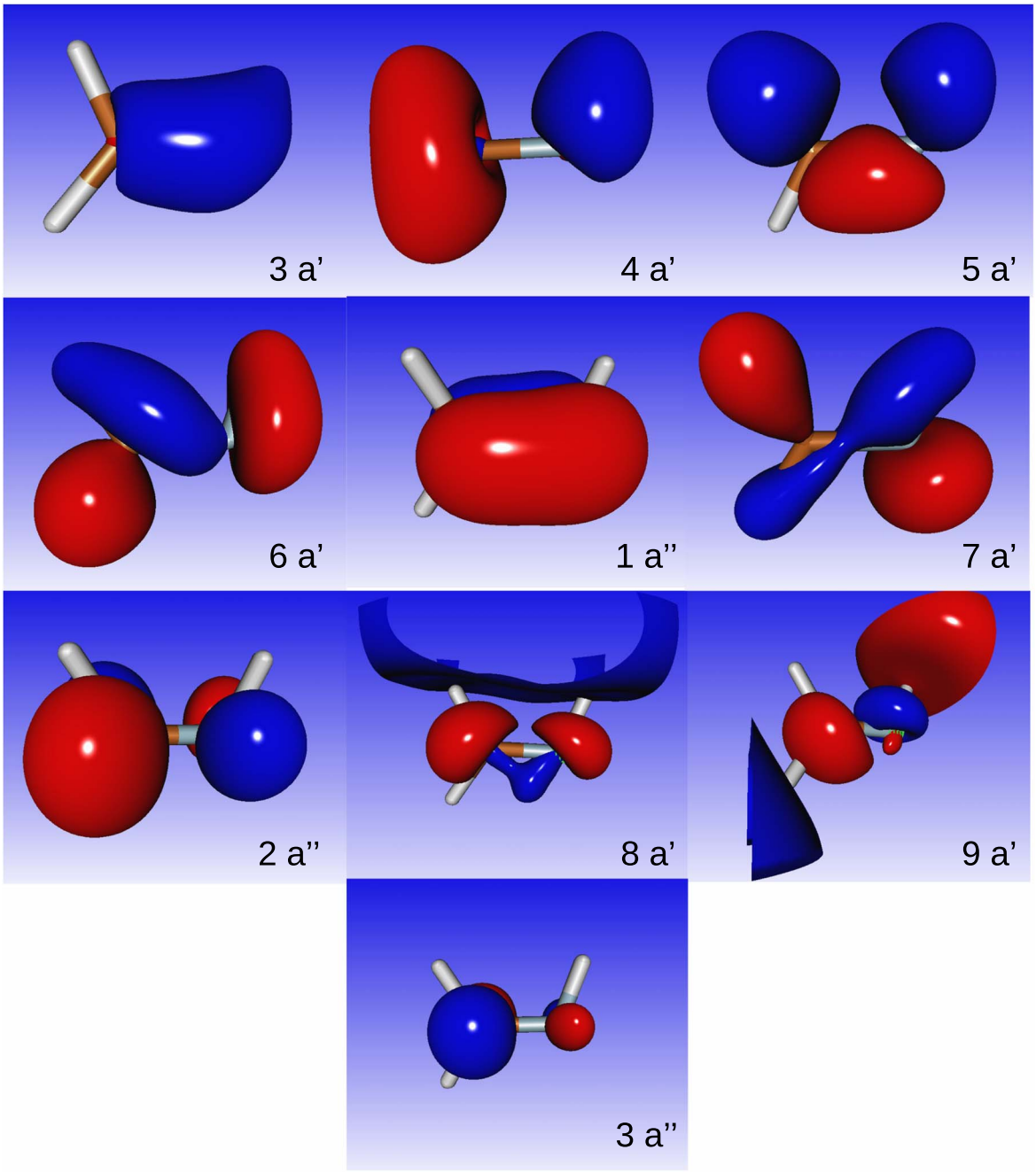

Figure 9. Representation of the CASSCF state-average orbitals included in the active space. It is noted that the full spatial extension of the Rydberg orbitals (8 a' and 9 a') cannot be captured due to their diffuse character.

ORCID iDs

A. Zanchet https://orcid.org/0000-0002-0471-5658
L. Bañares https://orcid.org/0000-0002-0777-2375
A. García-Vela https://orcid.org/0000-0002-1214-2132

References

Arenas, J. F., Marcos, J. I., Otero, J. C., Sánchez-Gálvez, A., & Soto, J. 1999, JChPh, 111, 551
Bock, H., & Dammel, R. 1987, Angew. Chem. Int. Ed. Engl., 26, 504
Bock, H., & Dammel, R. 1988, JAChS, 110, 5261
Bonacic-Koutecky, V., & Michl, J. 1985, AcTC, 68, 45
Bouallagui, A., Zanchet, A., Bañares, L., & García-Vela, A. 2022, PCCP, 24, 7387
Bruna, P. J., Krumbach, V., & Peyerimhoff, S. D. 1985, CaJCh, 63, 1594
Chandra, S., Sakshi, Sharma, M. K., & Kumar, N. 2016, InJPh, 90, 733
Chestnut, D. B. 2001, JCoCh, 22, 1702
Chicharro, D. V., Marggi Poullain, S., Zanchet, A., et al. 2019, Chem. Sci., 10, 6494
Chicharro, D. V., Zanchet, A., Bouallagui, A., et al. 2021, PCCP, 23, 2458
Cimiraglia, R., & Tomasi, J. 1977, JAChS, 99, 1135
Cuadrado, S., Goicoechea, J. R., Cernicharo, J., Fuente, A., Pety, J., & Tercero, B. 2017, A&A, 603, A124
Danger, G., Borget, F., & Chomat, M. 2011, A&A, 535, A47
Demuynck, J., Fox, D. J., Yamaguchi, Y., & Schaefer, H. F., III 1980, JAChS, 102, 6204
Dickens, J. E., Irvine, W. M., DeVries, C. H., & Ohishi, M. 1997, ApJ, 479, 307
Ditchfield, R., Del Bene, J. E., & Pople, J. A. 1972, JAChS, 94, 703
Dunning, T. H., Jr. 1989, JChPh, 90, 1007
Dutrey, A., Guilloteau, S., & Guelin, M. 1997, A&A, 317, L55
Duxbury, G., & Kato, H. 1981, FaDi, 71, 97

Godfrey, P. D., Brown, R. D., Robinson, B. J., & Sinclair, M. W. 1973, ApJL, 119, 13
Gorski, M. D., Aalto, S., Mangum, J., et al. 2021, A&A, 654, A110
Halonen, L., & Duxbury, G. 1985a, JChPh, 83, 2078
Halonen, L., & Duxbury, G. 1985b, JChPh, 83, 2091
Hamada, Y., Hashiguchi, K., Tsuboi, M., Koga, Y., & Kondo, S. J. 1984, JMoSp, 105, 70
Hirota, T., Yamamoto, S., Mikami, H., & Ohishi, M. 1998, ApJ, 503, 717
Jacox, M. E., & Milligan, D. E. 1975, JMoSp, 56, 333
Kastner, J. H., Zuckerman, B., Weintraub, D. A., & Forveille, T. 1997, Sci, 277, 67
Kitaura, K., Osamura, Y., & Nishimoto, K. 1978, CPL, 55, 531
Knowles, P. J., & Werner, H.-J. 1992, AcTC, 84, 95
Larson, C., Ji, Y., Samartzis, P., et al. 2006, JChPh, 125, 133302
Lavvas, P., Galand, M., Yelle, R. V., et al. 2011, Icar, 213, 233
Lavvas, P., Yelle, R. V., & Vuitton, V. 2009, Icar, 201, 626
Lavvas, P. P., Cousternis, A., & Vardavas, J. M. 2008, P&SS, 56, 67
Liszt, H., & Lucas, R. 2001, A&A, 370, 576
Loughnane, R. M., Redman, M. P., Thompson, M. A., et al. 2012, MNRAS, 420, 1367
MaCaulay, R., Burnelle, L. A., & Sandorfy, C. 1973, AcTC, 29, 1
Marconi, A., Testi, L., Natta, A., & Walmsley, C. M. 1998, A&A, 330, 696
Marggi Poullain, S., Chicharro, D. V., Zanchet, A., et al. 2019, PCCP, 21, 23017
Marggi Poullain, S., Rubio-Lago, L., Chicharro, D. V., et al. 2022, MolPh, 120, e1984598
McPherson, D. W., McKee, K. L., & Shevlin, P. B. 1983, JAChS, 105, 6193
Milligan, D. E. 1961, JChPh, 35, 1491
Nguyen, M. T. 1985, CPL, 117, 290
Nguyen, M. T., Sengupta, D., & Ha, T. K. 1996, JPhCh, 100, 6499
Orozco-Gonzalez, Y., Coutinho, K., Peon, J., & Canuto, S. 2012, JChPh, 137, 054307
Osamura, Y., Kitaura, K., Nishimoto, K., & Yamabe, S. 1979, CPL, 63, 406
Pearson, R., & Lovas, F. J. 1977, JChPh, 66, 4149
Peel, J. B., & Willet, G. D. 1975, J. Chem. Soc. Faraday Trans., 2, 1799
Pople, J. A., Raghavachari, K., Frisch, M. J., et al. 1983, JAChS, 105, 6389
Qin, S.-L., Wu, Y., Huang, M., et al. 2010, ApJ, 711, 399
Richards, C., Jr., Meredith, C., Kim, S.-J., Quelch, G. E., & Schaefer, H. F, III 1994, JChPh, 100, 481
Roithova, J., Schröder, D., & Schwarz, H. 2005, EurJOC, 2005, 3304
Sumathi, R. J. 1996, JMoSt, 364, 97
Tenenbaum, E. D., Dodd, J. L., Milam, S. N., Woolf, N. J., & Ziurys, L. M. 2010, ApJL, 720, L102
Teslja, A., Nizamov, B., & Dagdigian, P. J. 2004, JPCA, 108, 4433
Turner, B. E., Pirogov, L., & Minh, Y. C. 1997, ApJ, 483, 235
Turner, B. E., Terzieve, R., & Herbst, E. 1999, ApJ, 518, 699
Vuitton, V., Dutuit, O., Smith, M., & Balucani, N. 2014, in Titan: Interior, Surface, Atmosphere, and Space Environment, ed. I. Müller-Wodarg et al. (Cambridge: Cambridge Univ. Press), 224
Vuitton, V., Yelle, R. V., & McEwan, M. J. 2007, Icar, 191, 722
Werner, H.-J., & Knowles, P. J. 1985, JChPh, 82, 5053
Werner, H.-J., Knowles, P. J., Knizia, G., et al. 1996, MolPh, 89, 645
White, G. J., Araki, M., Greaves, J. S., Ohishi, M., & Higgin-Bottom, N. S. 2003, A&A, 407, 589
Zhou, C., Frigge, R., Turner, A. M., et al. 2019, PCCP, 21, 1952
Zhou, J., & Schlegel, H. B. 2009, JPCA, 113, 9958